

Conformational Changes in the Nicotinic Acetylcholine Receptor during Gating and Desensitization[†]

Innocent H. Yamodo,^{‡,⊥} David C. Chiara,^{||,⊥} Jonathan B. Cohen,^{||} and Keith W. Miller^{*,‡,§}

[‡]Department of Anesthesia, Critical Care and Pain Medicine, Massachusetts General Hospital, Boston, Massachusetts 02114, [§]Department of Biological Chemistry and Molecular Pharmacology, and ^{||}Department of Neurobiology, Harvard Medical School, Boston, Massachusetts 02115. [⊥]These authors contributed equally to this work.

Received September 4, 2009; Revised Manuscript Received December 3, 2009

ABSTRACT: The nicotinic acetylcholine receptor (nAChR) is a member of the important Cys loop ligand-gated ion channel superfamily that modulates neuronal excitability. After they respond to their agonists, their actions are terminated either by removal of ligand or by fast and slow desensitization, processes that play an important role in modulating the duration of conducting states and hence of integrated neuronal behavior. We monitored structural changes occurring during fast and slow desensitization in the transmembrane domain of the *Torpedo* nAChR using time-resolved photolabeling with the hydrophobic probe 3-(trifluoromethyl)-3-(*m*-iodophenyl)diazirine (TID). After channel opening, TID photolabels a residue on the δ -subunit's M2–M3 loop and a cluster of four residues on δ M1 and δ M2, defining an open state pocket [Arevalo, E., et al. (2005) *J. Biol. Chem.* 280, 13631–13640]. We now find that photolabeling of this pocket persists during the transition to the fast desensitized state, the extent of photoincorporation decreasing only with the transition to the slow desensitized state. In contrast, the extent of photoincorporation in the channel lumen at the conserved 9'-leucines on the second transmembrane helix (M2-9') decreased successively during the resting to open and open to fast desensitized state transitions, implying that the local conformation is different in each state, a conclusion consistent with the hypothesis that there are separate gates for channel opening and desensitization. Thus, although during fast desensitization there is a conformation change in the channel lumen at the level of M2-9', there is none in the regions of the δ -subunit's M2–M3 loop and the interior of its M1–M4 helix bundle until slow desensitization occurs.

The Cys loop ligand-gated ion channel superfamily, which includes nicotinic acetylcholine receptors (nAChRs),¹ 5-hydroxytryptamine type 3 (5-HT₃) receptors, γ -aminobutyric acid type A (GABA_A) receptors, and glycine receptors, has been studied intensively. These channels modulate synaptic and extrasynaptic neuronal excitability in response to their agonists, and their actions are terminated either by removal of the ligand or by desensitization, a process that plays an important role in modulating the duration of ligand-gated conducting states and hence of integrated neuronal behavior (1–3). A primary challenge is to understand not only how agonist binding in the extracellular ligand-binding domain (LBD) triggers a conformation change that opens an ion pore at a gate some 50 Å distant in the

transmembrane domain (TMD) but also how the channel then closes and the receptor is desensitized. Understanding channel opening has been aided by crystallographic structures of the LBD from homologous molluscan acetylcholine binding proteins (reviewed in ref 4) and a cryoelectron microscopy structure of the *Torpedo* acetylcholine receptor in the absence of agonist in the resting, closed state (5). Promisingly, two homologous prokaryotic channels have been crystallized recently (6–8), one of which may be in the open state; however, these channels do not desensitize, and there is no structure at comparable resolution of the desensitized state.

In contrast to the progress made in studies of channel opening (9–13), the structural basis of desensitization is poorly understood. Auerbach and Akk have proposed a two-gate model (14) in which there are structurally distinct activation and desensitization gates, a hypothesis that is supported by other lines of evidence (15, 16). Others have suggested that each subunit has only one desensitized structure and that the difference between fast and slow desensitization is merely in the number of subunits in the desensitized state (17). The LBD–TMD interface is implicated in desensitization because mutations therein affect the open channel lifetime and rate of desensitization in parallel (18).

An underlying problem with studying desensitized states is that they are nonconducting, and electrophysiological experiments infer their existence indirectly from the kinetics of the disappearance and reappearance of conducting states. The muscle type

[†]This research was supported by a grant from the National Institutes of Health (GM-58448), by the Department of Anesthesia and Critical Care, Massachusetts General Hospital, and by an award to the Harvard Medical School from the Howard Hughes Biomedical Research Support Program.

*To whom correspondence should be addressed: Department of Anesthesia, Critical Care and Pain Medicine, Massachusetts General Hospital, 32 Fruit St., Boston, MA 02114. Telephone: (617) 726-8985. Fax: (617) 724-8644. E-mail: k_miller@helix.mgh.harvard.edu.

¹Abbreviations: Carbachol, carbamylcholine; EndoLys-C, endoprotease Lys-C; HPLC, high-pressure liquid chromatography; LBD, ligand-binding domain; nAChR, nicotinic acetylcholine receptor; OPA, *o*-phthalaldehyde; PAGE, polyacrylamide gel electrophoresis; PTH, phenylthiohydantoin; SDS, sodium dodecyl sulfate; TID, 3-(trifluoromethyl)-3-(*m*-iodophenyl)diazirine; TMD, transmembrane domain; TPS, *Torpedo* physiological saline; V8 protease, *Staphylococcus aureus* endopeptidase Glu-C.

nAChR occurs in such abundance in *Torpedo* electroplaques that the application of complementary kinetic techniques that are not dependent on ion conduction has been possible. For example, fluorescence techniques have been employed to probe agonist-induced conformational changes using agonist site and noncompetitive inhibitor site probes (19, 20). This receptor is particularly convenient for probing conformational changes because the rates of opening, fast desensitization, and slow desensitization ensure that the peak occurrence of each successive state is well separated in time from the others (21–23); for example, see Figure 4b in ref 23.

Time-resolved photolabeling has also been used to probe agonist-induced conformational changes (24–28). It has a resolution in the millisecond range, well suited to probing conformational changes as the receptor progresses from the open state through the desensitized states. We have used time-resolved photolabeling with the hydrophobic photolabel 3-(trifluoromethyl)-3-(*m*-iodophenyl)diazirine (TID) to systematically probe structural changes on transient states of the nAChR. Within 1.5 ms of activation by rapid addition of agonist, a novel group of residues were robustly photolabeled (28). These residues, which were not detected in the equilibrium resting states, we termed activation-dependent to distinguish them from those channel lumen residues that are efficiently photolabeled in both the resting and open states. The former residues were located both at the extracellular end of the TMD of the δ -subunit between transmembrane helices δ M1 and δ M2 and in the interface between the TMD and LBD on the extracellular δ M2–M3 loop (Ile-288). This study aims to determine the phase of desensitization during which this structural change is reversed and whether similar conformational changes could be detected on other nAChR subunits.

EXPERIMENTAL PROCEDURES

Materials. nAChR-enriched membranes were isolated from *Torpedo californica* electric organs as described previously (29). The final membrane suspension was stored at -80°C in 38% sucrose and 0.02% NaN_3 under argon. The specific activity of the binding sites was determined using a [^3H]acetylcholine (PerkinElmer Life Sciences) binding assay and estimated to be 0.5–2.1 nmol of acetylcholine sites per milligram of protein as determined by the micro-BCA assay (Pierce). 3-(Trifluoromethyl)-3-(*m*-[^{125}I]iodophenyl)diazirine ([^{125}I]TID, 10 Ci/mmol) was obtained from GE Healthcare (Buckinghamshire, U.K.). Endoproteinase Lys-C (EndoLys-C), a lysine-specific protease, was obtained from Roche Applied Science, and *Staphylococcus aureus* endopeptidase Glu-C (V8 protease), a glutamate-specific protease, was from MP Biochemicals. TPCK-treated trypsin, which is specific for lysine and arginine, was from Worthington Biochemical Corp. (Freehold, NJ). All HPLC solvents were HPLC grade. *Torpedo* physiological saline (TPS) contains 250 mM NaCl, 5 mM KCl, 2 mM MgCl_2 , 5 mM sodium phosphate (pH 7.0), and 0.02% NaN_3 .

Time-Resolved Photolabeling of nAChR-Enriched Membranes. The method used was previously described (27, 28). Briefly, the loop of one of the two six-way sample valves was filled with 0.5 mL of nAChR-enriched membranes (4 mg of protein/mL) equilibrated with 7 μM [^{125}I]TID. The other six-way sample valve's loop was filled with 0.5 mL of 20 mM carbamylcholine (carbachol). The contents of the loops were forced through the mixer by a pneumatic ram, and after a designated

incubation time, the mixed samples were expelled onto a rotating stainless steel disk (60 rpm) precooled in liquid nitrogen, where they were instantaneously (<1 ms) frozen in a thin film. Incubation times were varied by changing the velocity of the ram and the lengths of the aging tube. The freeze-quenched samples were then irradiated (Black-Ray UV lamp, model UVL-56) for 30 min at 366 nm at a distance of ~ 3 cm on the slowly rotating disk (3 rpm) in contact with liquid nitrogen. For the equilibrium condition (slow desensitized state), the nAChR-enriched membranes at 2 mg/mL were equilibrated with 3.5 μM [^{125}I]TID and 10 mM Carbachol and incubated for 1 h. Both loops of the two six-way valves were filled with 0.5 mL of this mixture and treated as previously described. To isolate nAChR subunits on a scale appropriate for the identification of photolabeled amino acids by Edman degradation (preparative photolabeling), six to eight samples per condition were obtained and pooled. An aliquot of each freeze-quenched sample was saved for protein concentration determination and for counting on a gamma counter.

SDS–PAGE. To evaluate the reproducibility of the subunit photolabeling in the multiple samples collected for each preparative photolabeling condition, an aliquot of each frozen sample was thawed in sample buffer and resolved by SDS–PAGE. The polypeptides from each sample were visualized by Coomassie blue stain, and the labeled bands of interest were detected within the wet gel by phosphorimaging (2 h exposure at 25°C) using a Storm PhosphorImager (Amersham Biosciences). The samples from each labeling condition were then pooled, separated by SDS–PAGE, and analyzed with a phosphorimager as described above. To accommodate the excessive volume resulting from pooling up to eight freeze-quenching runs, each containing ~ 1 mL, special gels with deep wells (6–8 cm) and extended stacking gels (4 cm) were used. The resulting phosphorimages were used as a template to excise the subunits of interest. For the α -subunit, the excised bands were used for an “in gel” proteolytic digestion (see below). For the other subunits, the subunit bands were eluted passively for 3 days at room temperature in 12 mL of elution buffer [100 mM NH_4HCO_3 , 0.1% SDS, and 2.5 mM dithiothreitol (pH 8.4)], filtered, concentrated in Vivaspin 15 mL concentrators (Vivascience, Inc., Edgewood, NY), and precipitated in 75% acetone (>12 h at -20°C). The precipitates were resuspended overnight in 200 μL of resuspension buffer [15 mM tris(hydroxymethyl)aminomethane, 0.5 mM EDTA, and 0.1% SDS (pH 8.1)] at room temperature.

Proteolytic Digestion. Labeled subunits were digested with specific endoproteases. For the α -subunits, the excised bands were digested in gel with the V8 protease as previously described (30). After the electrophoresis, the mapping gels were stained with GelCode Blue stain (Pierce) and proteolytic fragments of 20 kDa (α V8–20), beginning at α Ser-173 and containing the M1, M2, and M3 transmembrane helices, were excised and recovered as described above. Both α V8–20 and an aliquot of the recovered δ -subunit were digested with EndoLys-C (0.75 unit) in resuspension buffer for 2 weeks at room temperature. The α V8–20 digests were fractionated using reversed phase HPLC. The δ -subunit digests were fractionated by Tricine SDS–PAGE (28), and the ^{125}I band of 10–14 kDa, which was identified by phosphorimaging, was excised and recovered as described above. Aliquots of the δ -subunit were also digested for 3 days with V8 protease (100%, w/w), and the digests were fractionated by reversed phase HPLC. Aliquots of the β -subunit were digested with trypsin (w/w) via addition of 4 volumes of

digestion buffer [50 mM NH_4HCO_3 and 0.5% Genapol C-100 (pH 8.1)] followed after 10 min by 0.1 volume of trypsin in 20 mM CaCl_2 .

Reversed Phase HPLC. The proteolytic fragments of the nAChR subunits were purified on an Agilent series 1100 HPLC system with an inline degasser and column heater. The purifications were achieved at 40 °C using a Brownlee Aquapore C-4 column (100 mm \times 2.1 mm, 7 μm particle size) with a C-2 guard column. The aqueous phase (solvent A) was 0.08% trifluoroacetic acid; the organic phase (solvent B) consisted of 60% acetonitrile, 40% 2-propanol, and 0.05% trifluoroacetic acid, and the gradients are included in the HPLC plots as dashed lines. The elution of peptides was monitored by the absorbance at 215 nm (Spectroflow 757, Kratos Analytical). The flow rates were 0.2 mL/min, and fractions of 0.5 mL were collected. All HPLC solvents were HPLC grade.

Sequence Analysis. Most HPLC fractions of interest were pooled and drop-loaded onto Biobrene-treated glass fiber filters at 45 °C. Fractions containing either αM4 or δM1 were absorbed onto a PVDF filter using the ProSorb absorption system (Applied Biosystems, Foster City, CA) following the manufacturer's procedure. N-Terminal sequence analysis of isolated nAChR subunit fragments was performed using an Applied Biosystems Procise 492 protein sequencer modified such that five-sixths of each cycle was collected for gamma counting and the other one-sixth was used for amino acid analysis. The number of picomoles of phenylthiohydantoin (PTH)-derivatized amino acids in each cycle was determined by chromatographic peak heights. The initial amount (I_0) and the repetitive yield (R) for detected peptides were determined by a nonlinear least-squares fit (Sigma Plot, Jandel Scientific) of the equation $f(x) = I_0R^x$, where $f(x)$ is the number of picomoles of the amino acid in cycle x . Because of known problems with quantifying their PTH derivatives, serines, histidines, tryptophans, and cysteines, although they were plotted, were omitted from the fit. The efficiency of photoincorporation of [^{125}I]TID into a specific residue in cycle x was determined by the equation $(\text{cpm}_x - \text{cpm}_{x-1})/5 \times I_0R^x$. For some samples, sequencing was interrupted and the material on the filter was treated with *o*-phthalaldehyde (OPA) as described previously (31, 32). OPA reacts with primary amines preferentially over secondary amines (i.e., proline) and may be used at any sequencing cycle to block Edman degradation of peptides not containing an N-terminal proline. The counts per minute detected in each cycle of Edman degradation was back-corrected for ^{125}I decay to the date of labeling.

Although the output from the Edman analysis in counts per minute per picomole is quantitative, there are many variables that may introduce errors during the time-resolved photolabeling, digestion, and purification steps. An analysis of errors in this and our previous time-resolved work, excluding data with <4 cpm/pmol, shows that the average standard deviation is $28 \pm 16\%$ (SD) of the mean counts per minute per picomole.

RESULTS

Experimental Strategy. We focused on conformation changes in three domains: the center of the pore around M2-9', the region contralateral to the pore at the extracellular end of M2 (18' and 22'), and the M2–M3 loop. We chose photolabeling times to coincide with peaks in the populations of the resting, open, fast desensitized and slow desensitized states based on evidence from rapid agonist-induced cation flux and fluorescent

agonist binding in *Torpedo* acetylcholine receptor rich vesicles (22, 23, 33). When the agonist binds, the resting state receptors convert to the open state in tens of microseconds (34). Passage to the fast desensitized state takes place with a time constant of ~ 150 – 300 ms and is complete by 1 s, while that to the slow desensitized state is complete in tens of seconds (23). Our experiments focused on changes occurring between pairs of states because at none of the four time points examined will all the receptors be in a single state. For example, in the absence of agonist, the resting state is in equilibrium with some 15% of receptors that are desensitized (19). This desensitized state is poorly photolabeled by TID, and its population does not change significantly in the first second after addition of agonist; therefore, it may be ignored when considering changes in photolabeling with time. Furthermore, studies with a fluorescent agonist suggest that TID does not significantly perturb the kinetics of desensitization (35), and this is confirmed in electrophysiological studies (28).

We determined the relative change in photoincorporation of [^{125}I]TID into nAChRs for three agonist-induced conformation changes: resting to open, open to fast desensitized, and fast desensitized to slow desensitized. The two conformations associated with each state transition were photolabeled on the same day under the same conditions, except for the time of incubation with agonist, and were subsequently processed in parallel. For the δ -subunit, we were interested in changes during all these transitions, whereas for the other subunits, we concentrated on the first two because at the subunit level there is no change between the fast and slow desensitized states (28). Although conformations may coexist (see above), we use the terms open, fast desensitized, and slow desensitized to refer to receptors photolabeled after exposure to 10 mM carbachol for 10–15 ms, 1 s, and 1 h, respectively. In all cases, the membranes were pre-equilibrated with TID.

Photolabeling in the δM2 Helix and δM2 – δM3 Loop. For each photolabeling condition, we isolated for sequence analysis the δ -subunit fragment that begins at $\delta\text{Met-257}$, the N-terminus of δM2 (termed $\delta\text{M2-1}'$) and extends through δM3 . The fragment was isolated from an EndoLys-C subunit digest by Tricine SDS–PAGE and reversed phase HPLC (28). The HPLC fractionations for the three state transitions are shown in Figure S1A–C of the Supporting Information (S denoting Supporting Information), and the sequencing results are given in the three sections below. For each photolabeling experiment, the efficiency of [^{125}I]TID photoincorporation at an individual position was quantified (in counts per minute per picomole) to compare labeling at other positions within the fragment from the same sample and from the second labeling condition performed in parallel.

(i) **Resting to Open State Transition.** To confirm our previous data for this state transition (28) and provide a point of comparison, the peptide isolated by HPLC as shown in Figure S1A and beginning at $\delta\text{Met-257}$ was subjected to 25 cycles of Edman degradation. The major photoincorporation in the pore region was at $\delta\text{M2-9}'$ Leu-265 (Figure 1A) with minor labeling at $\delta\text{M2-13}'$ Val-269 and $\delta\text{M2-16}'$ Leu-272. In agreement with our previous work, the efficiency of incorporation of [^{125}I]TID at Leu-265 decreased approximately 2-fold between the resting and open states, from 115 to 68 cpm/pmol.

Upon the transition to the open state, photoincorporation was observed into two additional residues located contralateral to the channel lumen (cycles 18 and 22). These residues, $\delta\text{M2-18}'$

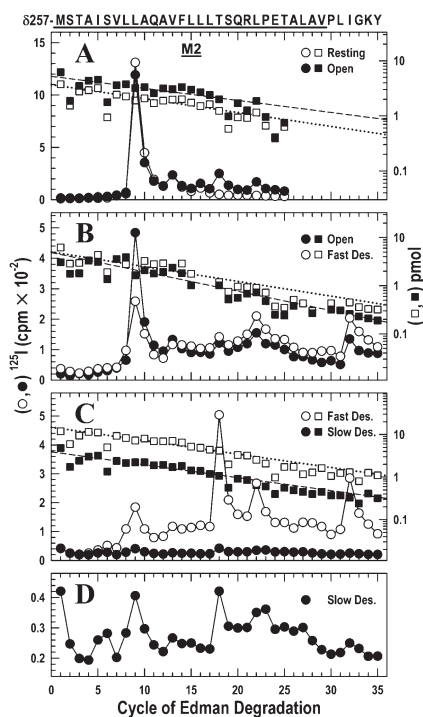


FIGURE 1: Photoincorporation of [^{125}I]TID into the $\delta\text{M}2$ helix and $\delta\text{M}2$ – $\text{M}3$ loop in the resting, open, fast desensitized, and slow desensitized states of *Torpedo* nAChR. nAChR-enriched membranes (4 mg/mL) were equilibrated with 7 mM [^{125}I]TID and then rapidly mixed with an equal volume of buffer (resting) or agonist (Carbachol, 20 mM; 10 mM final concentration) for 15 ms (open state), 1 s (fast desensitized state), or ≥ 1 h (slow desensitized state), then frozen in < 1 ms, and finally photolabeled for 30 min (see Experimental Procedures). In each case, the fragment beginning at δMet -257 was isolated from EndoLys-C digests of δ -subunits by SDS–PAGE and reversed phase HPLC as described in Experimental Procedures (Figure S1). The panels show ^{125}I (\circ and \bullet , left axis) and PTH-amino acids (\square and \blacksquare , right axis) released during the sequencing of δ -subunit peptides. The sequence beginning at the N-terminus of $\delta\text{M}2$ at Met-257 is shown at the top with the M2 transmembrane helix highlighted with a dark bar. (A) nAChRs were photolabeled in the resting (\circ and \square) and open (\bullet and \blacksquare) states. For sequencing the resting and open state samples, 9230 and 16140 cpm of ^{125}I were loaded onto filters, respectively. The primary sequence began at δMet -257 ($\delta\text{M}2$ -1') [(\square) $I_0 = 3.7$ pmol, and $R = 94\%$; (\blacksquare) $I_0 = 5.2$ pmol, and $R = 95\%$], with a secondary sequence beginning at δAsn -437 in both samples at ~ 0.3 pmol. Peaks of ^{125}I release (\circ and \bullet) were detected in the resting state at cycles 9, 13, and 16 and in the open state at cycles 9, 13, 16, 18, and 22, corresponding to residues δLeu -265, δVal -269, δLeu -272, δThr -274, and δLeu -278, respectively. (B) nAChRs were photolabeled in the open (\bullet and \blacksquare) and fast desensitized (\circ and \square) states. For sequencing the open and fast desensitized state samples, 24021 and 28221 cpm of ^{125}I were loaded onto filters, respectively. The fragment beginning at δMet -257 was present [(\blacksquare) $I_0 = 4.9$ pmol, and $R = 91\%$; (\square) $I_0 = 5.0$ pmol, and $R = 93\%$] along with the fragment beginning at δAsn -437 at ~ 8 pmol in both samples, which contains the M4 helix beginning at cycle 20. Peaks of ^{125}I release were observed in both samples at cycles 9, 13, 18, 22, and 32. Residues in M4 are labeled inefficiently by TID (δSer -457 at δMet -467 at < 1 cpm/pmol) because they are at the lipid interface (37) and they do not contribute to the peaks of ^{125}I release observed here. (C) nAChRs were photolabeled in the fast (\circ and \square) and slow desensitized (\bullet and \blacksquare) states. For sequencing the fast desensitized and slow desensitized state samples, 15450 and 2370 cpm of ^{125}I were loaded onto filters, respectively. The primary sequence began at δMet -257 [(\square) $I_0 = 15$ pmol, and $R = 93\%$; (\blacksquare) $I_0 = 3.9$ pmol, and $R = 93\%$], with the fragment beginning at δAsn -437 also present at ~ 2 pmol in each sample. Peaks of ^{125}I release occurred in the same cycles as in panel B. (D) The data from panel C for the slow desensitized state are replotted on an expanded scale.

Thr-274 and $\delta\text{M}2$ -22' Leu-278, were labeled with similar efficiencies of 14 and 9 cpm/pmol, respectively, in the open state and not labeled in the resting state. This confirms our previous study (28).

(ii) *Open to Fast Desensitized State Transition.* As described above, the peptide beginning with δMet -257 was isolated (Figure S1B) and then subjected to 35 cycles of Edman degradation (Figure 1B). This state transition caused the extent of photoincorporation in the channel lumen to decrease 3-fold at $\delta\text{M}2$ -9' Leu-265, from 39 to 12 cpm/pmol.

In contrast, in the two residues contralateral to the channel lumen, the transition from the open to the fast desensitized state resulted in little change in photoincorporation: $\delta\text{M}2$ -18' Thr-274, 7 versus 5 cpm/pmol; and $\delta\text{M}2$ -22' Leu-278, 11 versus 11 cpm/pmol. The $\delta\text{M}2$ – $\text{M}3$ loop δIle -288 (cycle 32) behaved similarly (65 vs 48 cpm/pmol). The higher levels of photoincorporation in the $\delta\text{M}2$ – $\text{M}3$ loop versus $\delta\text{M}2$ were observed previously in the open state (28).

(iii) *Fast to Slow Desensitized State Transition.* Following the procedures described above, the peptide beginning with δMet -257 was isolated (Figure S1C) and sequenced (Figure 1C). In the two residues contralateral to the channel lumen and the one in the $\delta\text{M}2$ – $\text{M}3$ loop, the transition from the fast to the slow desensitized state was accompanied by a marked decrease in the level of photoincorporation: $\delta\text{M}2$ -18' Thr-274, 19 versus 3 cpm/pmol; $\delta\text{M}2$ -22' Leu-278, 8 versus 1 cpm/pmol; and $\delta\text{M}2$ – $\text{M}3$ loop δIle -288, 24 versus 2 cpm/pmol. Although the decrease in the level of photoincorporation is nearly 1 order of magnitude, the pattern of photoincorporation in the slow desensitized state is seen to be similar to that in the fast desensitized state when displayed with an expanded scale (Figure 1D). Thus, the rapid structural changes that took place in these regions of the nAChR during channel opening and that remained present in the fast desensitized state are finally reversed when the slow desensitized state is attained tens of seconds later, but the pattern is distinct from that in the resting state.

Within the lumen of the ion channel ($\delta\text{M}2$ -9'), the level of photoincorporation was so low (2 and 1 cpm/pmol for the fast and slow desensitized states, respectively) that we hesitate to draw a conclusion. The low level of release at cycle 9 in the fast desensitized state is likely anomalous (compare to Figure 1B). Furthermore, release later in the same sequencing run at cycle 32 (δIle -288) was normal and is independently corroborated in Figure 2C.

Photolabeling in the $\delta\text{M}2$ – $\delta\text{M}3$ Loop and $\delta\text{M}3$ Helix. To provide a more complete characterization of the state dependence of photolabeling in the $\delta\text{M}2$ – $\delta\text{M}3$ loop and to characterize labeling within $\delta\text{M}3$, the δ -subunit was digested with V8 protease, which cleaves at δGlu -280, and the digest was fractionated by reversed phase HPLC (36). Although the hydrophobic HPLC fractions with photoincorporated ^{125}I (Figure S2A) include other hydrophobic fragments containing $\delta\text{M}1$, $\delta\text{M}2$, and $\delta\text{M}4$, these can be N-terminally blocked by being treated with OPA, as described above, after the fifth cycle, leaving only the δThr -281 fragment, now starting at δPro -286, to be sequenced (31, 36). The advantage of this strategy is that δIle -288 is assayed as the third residue after the OPA treatment rather than as the 32nd residue of the sequencing run as in the samples digested with EndoLys-C (Figure 1). The results are given in the three following sections.

(i) *Resting to Open State Transition.* In the open state sample, there was a single sharp ^{125}I release in the eighth cycle

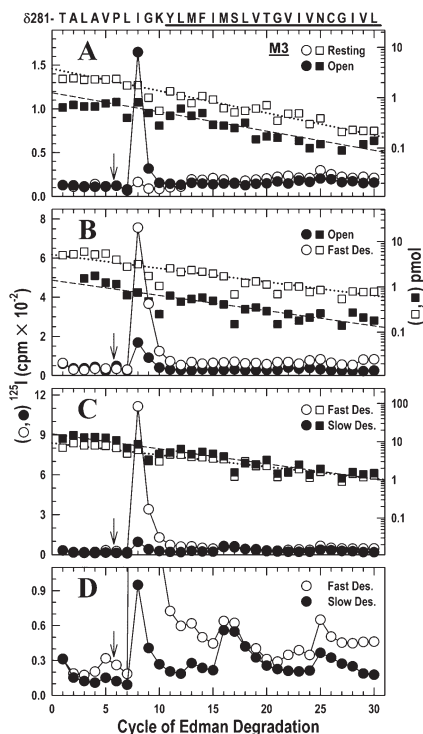


FIGURE 2: Photoincorporation of [^{125}I]TID in the $\delta\text{M2-M3}$ loop and δM3 helix in the resting, open, fast, and slow desensitized states of the *Torpedo* nAChR. Photolabeled nAChRs were from the experiments described in the legend of Figure 1. The panels show ^{125}I (\circ and \bullet , left axis) and PTH-amino acids (\square and \blacksquare , right axis) released during the sequencing. The sequence of the δ -subunit fragment beginning at $\delta\text{Thr-281}$ ($\delta\text{M2-25}'$), near the C-terminus of δM2 and continuing through the $\delta\text{M2-M3}$ loop into δM3 (highlighted with a dark bar), is shown at the top. Aliquots of δ -subunits were digested in solution with V8 protease. The digests were fractionated by reversed phase HPLC from which fractions containing the desired peptide were pooled (Figure S2A–C) for sequencing. To restrict the sequencing to the fragment beginning at $\delta\text{Thr-281}$, each sequencing filter was treated with OPA after five cycles of Edman degradation (i.e., when $\delta\text{Pro-286}$ was the N-terminal residue) (\downarrow) to block other peptides that do not contain a proline at that cycle. (A) nAChRs were photolabeled in the resting (\circ and \square) and open (\bullet and \blacksquare) states. For sequencing the resting and open state samples, 4650 and 2750 cpm of ^{125}I were loaded onto filters, respectively. The fragment beginning at $\delta\text{Thr-281}$ was the only sequence remaining after the OPA treatment [$(\square) I_0 = 3.8$ pmol, and $R = 90\%$; $(\blacksquare) I_0 = 1.3$ pmol, and $R = 92\%$]. A prominent release of ^{125}I was detected in cycle 8 ($\delta\text{Ile-288}$) only in the open state sample. There were minor peaks of ^{125}I release in cycles 13 and 25 ($\delta\text{Met-293}$ and $\delta\text{Asn-305}$, respectively). (B) nAChRs were photolabeled in the open (\bullet and \blacksquare) and fast desensitized (\circ and \square) states. For sequencing the open and fast desensitized state samples, 6880 and 24263 cpm of ^{125}I were loaded onto filters, respectively. The fragment beginning at $\delta\text{Thr-281}$ was the only sequence remaining after the OPA treatment [$(\blacksquare) I_0 = 1.4$, and $R = 93\%$; $(\square) I_0 = 5.2$ pmol, and $R = 92\%$]. A prominent release of ^{125}I was detected in cycle 8 ($\delta\text{Ile-288}$) in the resting and fast desensitized state, with minor release occurring at cycles 13, 22, and 25 ($\delta\text{Met-293}$, $\delta\text{Val-302}$, and $\delta\text{Asn-305}$, respectively). (C) nAChRs were photolabeled in the fast (\circ and \square) and slow desensitized (\bullet and \blacksquare) states. For sequencing the fast desensitized and slow desensitized state samples, 23900 and 6850 cpm of ^{125}I were loaded onto filters, respectively. The fragment beginning at $\delta\text{Thr-281}$ was the only sequence remaining after the OPA treatment [$(\square) I_0 = 9.1$ pmol, and $R = 93\%$; $(\blacksquare) I_0 = 16$ pmol, and $R = 91\%$]. The prominent ^{125}I releases in cycle 8 ($\delta\text{Ile-288}$) in the fast desensitized state fell dramatically during slow desensitization. (D) Because the amount of peptide is higher in panel C than in panels A and B, the low level of photoincorporation in δM3 (cycles 13, 22, and 25; $\delta\text{Met-293}$, $\delta\text{Val-302}$, and $\delta\text{Asn-305}$, respectively) is clear when the data are plotted on an expanded axis.

(Figure 2A), consistent with incorporation of [^{125}I]TID into $\delta\text{Ile-288}$ on the $\delta\text{M2-M3}$ loop. The large magnitude of the photoincorporation (49 cpm/pmol) contrasts with the very weak labeling in the resting state (1 cpm/pmol), consistent with previous observations (28).

(ii) *Open to Fast Desensitized State Transition.* Sequence analysis (Figure 2B) revealed once again a single peak of ^{125}I release in the eighth cycle, corresponding to $\delta\text{Ile-288}$, but this time it was evident in both the open and fast desensitized states. After correction for the difference in the quantity of peptide being sequenced, the efficiency of photolabeling was similar in both states (38 and 53 cpm/pmol, respectively). This suggests that the structural change in the $\delta\text{M2-M3}$ loop initiated by opening remains present when the channel is closed by fast desensitization, consistent with the findings depicted in Figure 1B.

(iii) *Fast to Slow Desensitized State Transition.* The level of photoincorporation into $\delta\text{Ile-288}$ decreased dramatically upon slow desensitization from 43 to 2 cpm/pmol (Figure 2C), a low level similar to that in the resting state. Because a larger amount of peptide was sequenced in this run, the relatively inefficient labeling in cycles 13, 16, and 25 is evident when the data are replotted with an expanded scale (Figure 2D). Photoincorporation into these residues in the fast and slow desensitized states occurred at $\delta\text{Met-293}$ (0.1 and 0.4 cpm/pmol, respectively), $\delta\text{Met-296}$ (1 and 2 cpm/pmol, respectively), and $\delta\text{Asn-305}$ (4 and 2 cpm/pmol, respectively). The latter residue is also apparent in Figure 2A at comparable levels (6 and 5 cpm/pmol) for the resting and open states, respectively. The lack of clear state dependence is not unexpected because some of these residues were reported previously to be photolabeled by [^{125}I]TID from the lipid interface (37).

Comparison of Photolabeling of δM1 in the Fast and Slow Desensitized States. Our previous work established that two residues in the δM1 domain, $\delta\text{Phe-232}$ and $\delta\text{Cys-236}$, were photolabeled in the open but not the resting state (28). To determine if these residues behave synchronously with $\delta\text{M2-18}'$ Thr-274, $\delta\text{M2-22}'$ Leu-278, and Ile-288 in the $\delta\text{M2-M3}$ loop, we took advantage of the fact that the fragment beginning at $\delta\text{Phe-206}$ before δM1 can be isolated from the same HPLC fractionation (Figure S1C) of the EndoLys-C digest of the δ -subunit that yielded δM2 (28). A single peptide beginning at $\delta\text{Phe-206}$ in the N-terminal domain was sequenced for 19 cycles without ^{125}I release (Figure 3). Sequencing was stopped before $\delta\text{Pro-225}$, two residues before the beginning of δM1 , for OPA treatment, followed by 16 additional cycles of Edman degradation. Strong release of ^{125}I was observed in cycles 27 and 31 in the fast but not the slow desensitized state sample. The photoincorporation in the fast and the slow desensitized state occurred at $\delta\text{Phe-232}$ (29 and 2 cpm/pmol, respectively) and $\delta\text{Cys-236}$ (30 and 7 cpm/pmol, respectively). In a separate experiment (not shown), we confirmed that there is photoincorporation into $\delta\text{Phe-232}$ in the open state (24 cpm/pmol), as observed previously (28).

Comparison of Photolabeling of αM2 in the Resting and Open States. Next we asked whether the α -subunit contained residues equivalent to those in δM2 that are only labeled after activation. We therefore isolated for sequence analysis a fragment beginning at the N-terminus of αM2 ($\alpha\text{Met-243}$, $\alpha\text{M2-1}'$) by HPLC fractionation of an EndoLys-C digest of an ~ 20 kDa fragment beginning at $\alpha\text{Ser-173}$ that is produced when the α -subunit is digested with V8 protease (Figure S3) (see Experimental Procedures). Sequencing (Figure 4) revealed a peptide beginning at $\alpha\text{Met-243}$. Under both labeling conditions, there

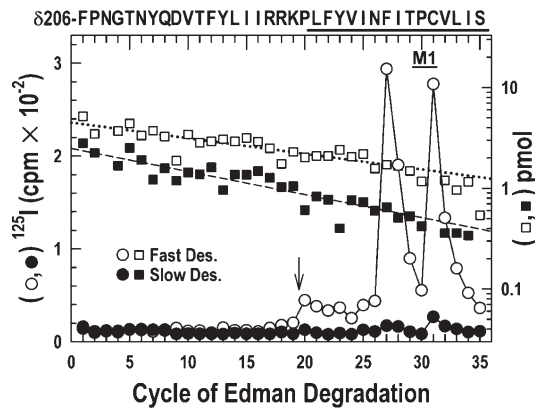


FIGURE 3: Photoincorporation of [125 I]TID into the δ M1 helix in the fast desensitized and slow desensitized states of nAChR. 125 I (\circ and \bullet) and PTH-amino acids (\square and \blacksquare) released during sequencing of the fragment beginning at δ Phe-206 and extending through δ M1, which was isolated by reversed phase HPLC fractionation of the EndoLys-C digests of the δ -subunit described in the legend of Figure 1 and Figure S1 from nAChRs photolabeled in the fast desensitized (\circ and \square) and slow desensitized (\bullet and \blacksquare) states. For sequencing the fast desensitized and slow desensitized state samples, 7600 and 840 cpm of 125 I, respectively, were loaded onto filters. To confirm that the 125 I release after cycle 20 could be attributed to δ M1, both samples were treated with OPA after 19 cycles of Edman degradation (i.e., when δ Pro-225 was the N-terminal residue) (\dagger) to prevent further sequencing of any other peptides in the samples not containing an N-terminal proline at that cycle. Even before the OPA treatment, however, the only sequence detected began at δ Phe-206 [\square] $I_0 = 4.5$ pmol, and $R = 97\%$; [\blacksquare] $I_0 = 2.5$ pmol, and $R = 95\%$]. Prominent labeling at cycles 27 and 31 was seen only in the fast desensitized state.

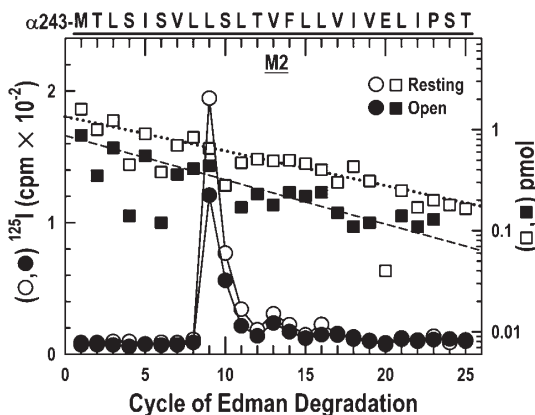


FIGURE 4: Photoincorporation of [125 I]TID into the α M2 helix in the resting and open states. 125 I (\circ and \bullet) and PTH-amino acids (\square and \blacksquare) released while sequencing the fragment beginning at α Met-243 (α M2-1'), which was isolated from the α -subunits photolabeled in the experiment described in the legend of Figure 1A by HPLC purification of an EndoLys-C digest (Figure S3) of a 20 kDa fragment produced by digestion with V8 protease. For sequencing the resting and open state samples, 2217 and 1874 cpm of 125 I, respectively, were loaded onto filters. Sequencing revealed a single peptide [for the resting state (\square), $I_0 = 1.3$ pmol and $R = 92\%$; for the open state (\blacksquare), $I_0 = 0.9$ pmol and $R = 90\%$]. A major peak of 125 I release was observed in cycle 9 (α Leu-251), with minor peaks at cycles 13 (α Val-255) and 16 (α Leu-258).

was a single robust peak of 125 I release at cycle 9 followed by two smaller ones at cycles 13 and 16, with photoincorporation efficiencies similar in the resting and open states: α M2-9' Leu-251 (57 and 64 cpm/pmol, respectively), α M2-13' Val-255 (5 and 8 cpm/pmol, respectively), and α M2-16' Leu-258 (4 and

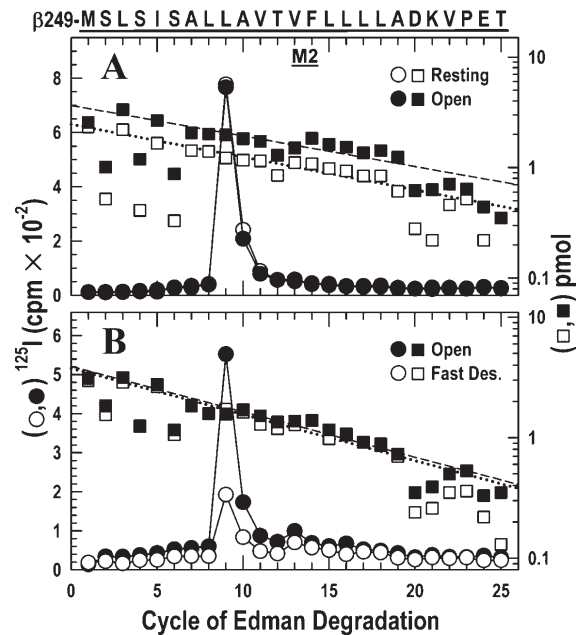


FIGURE 5: Photoincorporation of [125 I]TID into the β M2 helix in the resting, open, and fast desensitized states. 125 I (\circ and \bullet) and PTH-amino acids (\square and \blacksquare) released while sequencing the fragment beginning at β Met-249 (β M2-1'), which was isolated from the β -subunits photolabeled in the experiments described in the legend of Figure 1A,B by HPLC purification (Figure S4) of an ~ 10 kDa fragment isolated by Tricine SDS-PAGE from trypsin digests. (A) nAChRs were photolabeled in the resting (\circ and \square) and open (\bullet and \blacksquare) states. For sequencing the resting and open state samples, 4252 and 4523 cpm of 125 I, respectively, were loaded onto filters. Sequencing revealed a single peptide beginning at β Met-249 [\square] $I_0 = 2.5$ pmol, and $R = 93\%$; [\blacksquare] $I_0 = 3.6$ pmol, and $R = 94\%$]. There was a major peak of 125 I release in both states at cycle 9, corresponding to β Leu-257. (B) nAChRs were photolabeled in the open (\bullet and \blacksquare) and the fast desensitized (\circ and \square) states. For sequencing the open and fast desensitized state samples, 3166 and 1060 cpm of 125 I, respectively, were loaded onto filters. Sequencing revealed a single peptide beginning at β Met-249 [\blacksquare] $I_0 = 3.9$ pmol, and $R = 92\%$; [\square] $I_0 = 3.8$ pmol, and $R = 92\%$]. The major peak of 125 I release in both states was at cycle 9 (β Leu-257), with minor release at cycles 13 (β Val-261) and 16 (β Leu-264).

3 cpm/pmol, respectively). Thus, photoincorporation into the channel lumen of α M2 is not strongly affected by channel opening. There was no release of 125 I at cycle 18 or 22 in either sample.

Comparison of Photolabeling of β M2 in the Resting and Open States. To identify residues photolabeled by [125 I]TID, β -subunits of nAChR were digested with trypsin and a band of ~ 10 kDa was isolated and purified by HPLC (Figure S4A). A single peptide beginning with β Met-249 at the N-terminus of β M2 was detected with a single peak of 125 I release in cycle 9, corresponding to β M2-9' Leu-257. The levels of photoincorporation in this residue were 109 and 72 cpm/pmol for the resting and open states, respectively (Figure 5A). There was no release at cycle 18 or 22 in either sample.

Comparison of Photolabeling of β M2 in the Open and Fast Desensitized States. Using the procedure described in the preceding paragraph, 125 I release was observed in cycles 9 and 13 corresponding to the labeling of residues β M2-9' Leu-257 and β M2-13' Val-261 (Figure 5B). Photoincorporation efficiencies for the open versus the fast desensitized state for these two residues were as follows: 55 versus 19 cpm/pmol, respectively, and 4 versus 5 cpm/pmol, respectively. There was no release at cycle 18 or 22 in either sample.

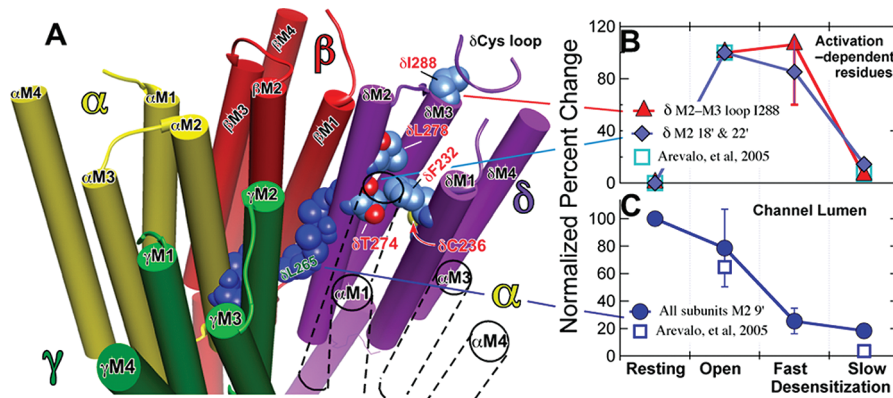


FIGURE 6: Location (A) and contrasting state dependence of the activation-dependent (B) and channel lumen (C) groups of residues. (A) A representation of the transmembrane region of the *Torpedo* nAChR based on the 2005 structure [Protein Data Bank entry 2gb9 (5)]. The receptor is viewed from the extracellular, N-terminal side, and the structure is sliced to show the transmembrane domain (TMD) only. The subunits are color-coded as follows (yellow for α , red for β , green for γ , and purple for δ ; the TMD of the second α -subunit that is situated between the γ - and δ -subunits is shown only in outline for the sake of clarity). The channel lumen residues are colored dark blue; the M2-9' residues are shown for each subunit and the M2-13' and M2-16' residues for the δ -subunit. The δ M2-9' Leu-265 is identified with green lettering. For the activation-dependent residues on the δ -subunit, the carbon atoms are colored corn blue, oxygens red, and nitrogens mid blue; residues are identified with red lettering. At the top right near δ Ile-288, a portion of the δ -subunit's Cys loop from the LBD is shown in ribbon representation. Molecular graphics were produced using the UCSF Chimera package from the Resource for Biocomputing, Visualization, and Informatics at the University of California (San Francisco, CA) (supported by National Institutes of Health Grant P41 RR-01081) (48). (B and C) Normalized efficiency of photoincorporation of [125 I]TID as the nAChR passes sequentially from the resting through the open and fast desensitized states to the slow desensitized state. (B) Biphasic state dependence of photoincorporation into the activation-dependent residues in the δ -subunit. The residues are identified in the key. The percent change in each pair of experiments was calculated. The data for δ M2-18' and δ M2-22' (Thr-274 and Leu-278) were grouped and averaged (two replicates per point). For the δ M2-M3 loop residue, Ile-288, there were two replicates for each state transition (Figures 1 and 2). The data were then normalized with error propagation to the open state, which was set to 100. There was no photolabeling in the resting state, equal degrees of photoincorporation in the open and fast desensitized states, and only modest photolabeling in the slow desensitized state. (C) State dependence of the efficiency of photoincorporation into the channel lumen M2-9' residues on the α -, β -, and δ -subunits (α M2 Leu-251, β M2 Leu-257, and δ M2 Leu-265, respectively). The data were analyzed as described for panel B. The percent change in each pair of experiments was calculated. We assumed 9'-leucine photoincorporation was equal in all subunits and averaged the data, which were then normalized with error propagation to the resting state, which was set to 100. For the sake of comparison, the squares show data from our previous study (28) for the mean of δ M2-18' and δ M2-22' normalized to the open state (B) and for δ M2 Leu-265 normalized to the resting state (C).

DISCUSSION

Location of the Photolabeled Residues. Using time-resolved photolabeling, we have followed structural changes as the nAChR passed from the open to the fast desensitized state and from that state to the slow desensitized state. Combined with our previous study on changes occurring during agonist-induced channel opening (28), the work covers a time span from 1.5 ms to many minutes after rapid addition of agonist. Our results are summarized in graphical form in Figure 6. TID photolabeling reported on structural changes in three distinct domains of the *Torpedo* nAChR. The first domain is the pseudocentrosymmetric subunit interface site in the channel lumen, predominantly at the conserved M2-9' leucines, α Leu-251, β Leu-257, and δ Leu-265, but also more extracellular at M2-13' and M2-16'. The photolabeling kinetics of the channel lumen residues are summarized in Figure 6C. The second domain is the interface between the ligand-binding domain (LBD) and the transmembrane domain. Here in the δ M2-M3 loop, the photolabeled δ Ile-288 makes contact with the conserved Cys loop of the LBD at the highly conserved δ Phe-137 and δ Pro-138 (Figure S5). The third domain is the extracellular end of the δ -subunit's transmembrane domain where we photolabeled two residues one turn apart both on M1 (δ Phe-232 and δ Cys-236) and on M2-18' and M2-22' (δ Thr-274 and δ Leu-278). On one side, these residues are bounded by the α -subunit- δ -subunit interface and on the other by the space within the δ -subunit's four-helix bundle (Figure 6A and Figure S5). In the second domain (δ M2-M3 loop), the α -carbon of δ Ile-288 is 13–20 Å from those of the residues on M1 and M2. Although structurally distinct, the photolabeling kinetics of the residues in the second and third domains were similar

(Figure 6B), and they may be considered together; we have previously termed them the activation-dependent residues and predicted that they all contribute to a single TID binding pocket (28).

An interesting spatiotemporal pattern of agonist-induced structural changes was observed to occur asynchronously over a wide time frame (Figure 6B, C). In our previous study, the efficiency of photoincorporation into the activation-dependent residues on the δ -subunit was similar at 1.5 and 10 ms following addition of agonist (28). Here we show that there is no further structural change during fast desensitization in this region. Thus, after the initial change detected 1.5 ms after addition of agonist, there is no further change until slow desensitization occurs. In contrast, in the channel lumen, structural changes were detected both during opening and during fast desensitization. Thus, during fast desensitization, structural changes occurring in the center of the channel lumen at M2-9' are uncoupled from those contralateral to the extracellular end of M2 and in the δ M2-M3 loop in contact with the LBD (compare panels B and C of Figure 6). However, upon slow desensitization, a major structural change occurs in the latter regions, while either modest or no changes are detected in the channel lumen. Finally, the slow desensitized state can be distinguished from the resting state, not only, as expected, in the center of the channel lumen but also in the two more extracellular domains where the efficiency of photolabeling in the activation-dependent residues remains higher in the slow desensitized state than in the resting state, a result in agreement with another recent study (38).

This microscopic pattern of photolabeling is consistent with that of the intact subunits (28). The δ -subunit is the only one to

experience an increase in the level of photoincorporation upon opening because it is the only one with photoincorporation in the activation-dependent residues and this offsets the decrease in the channel lumen. During fast desensitization, all subunits experience a decrease in the extent of photoincorporation originating in the channel lumen, but the level in the δ -subunit remains higher than in the other subunits. Finally, during slow desensitization, only the level of δ -subunit photoincorporation decreases sharply because photoincorporation in the activation-dependent residues is lost.

Relevance to Models of Gating and Desensitization. Our conclusion that the channel lumen's structure in the center of the M2 domain is different in the resting, open, and fast desensitized states is consistent with the two-gate model, which proposes an activation gate and a separate desensitization gate (14, 16, 28, 39). In each of the three states we studied, the model predicts a different arrangement of gates in the conduction pathway. In the resting state, the desensitization gate is open and the activation gate is closed. Activation opens the latter gate, and conduction occurs. During fast desensitization, the desensitization gate closes while the activation gate remains open.

The uncoupled model proposes that desensitization is not a concerted process, that each subunit has only one desensitized structure, and that the difference between fast and slow desensitization is merely in the number of subunits in the desensitized state (17). Supporting evidence comes from rapid kinetics studies with a fluorescent agonist that suggests that the agonist site at the α -subunit- δ -subunit interface desensitizes more slowly than that at the α -subunit- γ -subunit interface (40, 41), pointing to a model in which a conformation change at the α -subunit- γ -subunit interface accompanies fast desensitization and a similar one at the α -subunit- δ -subunit interface accompanies slow desensitization. Our demonstration that the activation-dependent residues on the δ -subunit change only during slow desensitization is consistent with this conclusion. Furthermore, the conformation at the α -subunit- δ -subunit agonist site and that at the extracellular end of the transmembrane domain of the δ -subunit appear to be tightly coupled both across the α -subunit- δ -subunit interface and across the LBD-TMD interface. At the same time, we observe changes in the centrosymmetric site in the channel lumen (δ M2-9' Leu-265), but it is likely that these reflect conformation changes in neighboring subunits rather than changes in the δ -subunit's conformation, although we cannot rule out the latter possibility.

Although many studies have demonstrated the importance of the M2-M3 loop in channel gating, few have considered desensitization. Recent electrophysiological studies of chimeras of two receptors with very different desensitization rates, the nACh α 7 receptor and 5HT_{3A}R, show that mutations in the M2-M3 loop affect the open channel lifetime and rate of desensitization in parallel (18). This is consistent with our observations on the δ -subunit. In addition, our results suggest that structural changes in the δ M2-M3 loop are rather rigidly coupled to those at the top of δ M2 and δ M1 because the levels of photolabeling of all five activation-dependent residues change in parallel. Comparison of the two prokaryotic structures suggests that gating involves a "tilting" of M2 pivoted on its central region so that the extracellular end moves counterclockwise around the pore's axis (viewed from the LBD) and outward toward M3, which in turn tilts outward. The tilting of M2 during opening would move δ M2 residues Thr-274 and Leu-278, which are contralateral to the channel lumen, into the pocket of the

δ -subunit that is bounded by the four-helix bundle and change the environment around δ Ile-288 on the δ M2-M3 loop. It is likely that these coupled motions are driven by the interaction of the Cys loop with the δ M2-M3 loop (see below). One possibility is that in the open state δ Ile-288 takes up a position on the surface of the same helix-bound pocket that has the other activation-dependent residues lining its surface (28). There are two arguments against this. First, δ Ile-288 is photolabeled more efficiently than the other residues, suggesting, but not proving, that they may not occupy the same pocket. Second, comparison of the two prokaryotic structures does not reveal such a rearrangement of the M2-M3 loop in this direction, although this argument is complicated by the different lengths of that loop in the two representative structures. Further discussion must await the determination of the structure of a single protein in the resting and open state.

Theoretical modeling provides some insights into the conformational dynamics in the region of the activation-dependent residues. Thus, a molecular dynamics normal-mode analysis study of the α 7 nAChR suggested a direct coupling between a twisting motion of the LBD and dynamic changes of M2 (42). The coupling occurred at the interface between the Cys loop and the M2-M3 loop. The conserved Phe-135 (δ Phe-137 in *Torpedo* numbering) is stabilized within a hydrophobic pocket formed by Leu-270 and Ile-271 (*Torpedo* δ -subunit numbering being Leu-287 and Ile-288, respectively; both subunits have a Pro-Leu-Ile sequence at the M3 end of the M2-M3 loop). The downward motion of the M2-M3 loop caused the M2 helices to tilt. However, our results refer to the δ -subunit which does not bind the agonist and is a so-called complementary subunit, contributing to agonist action at the α -subunit- δ -subunit interface. A theoretical study of the α 4 β 2 nAChR is of interest (43) because it found motions in the LBD-TMD interface similar to those in the study mentioned above and, in addition, that those in the complementary β -subunits were greater than those in the α -subunits.

Implications for Drug Action. This work, together with our previous study (28), has delineated the behavior of hydrophobic pockets through four conformations of the nAChR. It adds weight to the allosteric hypothesis of general anesthetic action that requires the existence of general anesthetic binding sites whose affinity varies with the protein's conformation. Furthermore, our work shows that more than one drug binding pocket can be occupied simultaneously in the nAChR TMD and that the binding properties of these pockets may depend on the protein's conformation in different ways, a conclusion that is supported by recent studies with TDBzl-etomidate, a photoreactive analogue of the general anesthetic etomidate (44).

The kinetic behavior of the δ -subunit's activation-dependent residues on M1 and M2 predicts that this four-helix bundle binding pocket, reminiscent of that hypothesized to be responsible for volatile anesthetic action on GABA_A receptors (45), has a similar structure in the open and fast desensitized states, but two different structures in the resting state and slow desensitized state. Nonetheless, the much smaller general anesthetic, halothane, does label the resting state at δ Tyr-228 (46), one helical turn above the activation-dependent residue δ Phe-232, illustrating the importance of an agent's size; the smaller halothane has access to the pocket that is denied to the bulkier TID in this conformation. Furthermore, consistent with our conclusion that the resting and slow desensitized states are not equivalent, halothane

photoincorporation is enhanced relative to the resting state by slow desensitization (46).

In the channel lumen at the level of the M2-9' residues and in the hydrophobic patch extracellular to these regions (M2-13' and M2-16'), the environment appears to be different in each of the conformations studied, and an agent binding here might have a different affinity for each state. On the extracellular side of the hydrophobic patch in the channel lumen at M2-20' (α Glu-262 and δ Gln-276), azietomidate, another photoactivatable analogue of the general anesthetic etomidate, labels ~2-fold more efficiently in the open state than in the slow desensitized state, suggesting more modest changes in this region (47).

CONCLUSIONS

We have provided new information about structural changes that take place during fast desensitization. Specifically, we have been able to probe a region at the extracellular end of the TMD of the δ -subunit. The structure here changes when the channel opens (28). The open state structure persists in the fast desensitized state, only changing again when the slow desensitized state is attained. At the same time in the channel lumen at the level of the conserved M2-9' leucines, the structures of the closed, open, and fast desensitized states are all different. Thus, the structures of the ion pore in the two nonconducting states (resting and fast desensitized) connected to the open state are not equivalent.

ACKNOWLEDGMENT

We thank Z. Dostalova for help in preparing acetylcholine receptor rich *Torpedo* membranes.

SUPPORTING INFORMATION AVAILABLE

HPLC purification of labeled peptides and a molecular model. This material is available free of charge via the Internet at <http://pubs.acs.org>.

REFERENCES

- Cederholm, J. M., Schofield, P. R., and Lewis, T. M. (2009) Gating mechanisms in Cys-loop receptors. *Eur. Biophys. J.* 39, 37–49.
- Sine, S. M., and Engel, A. G. (2006) Recent advances in Cys-loop receptor structure and function. *Nature* 440, 448–455.
- Giniatullin, R., Nistri, A., and Yakel, J. L. (2005) Desensitization of nicotinic ACh receptors: Shaping cholinergic signaling. *Trends Neurosci.* 28, 371–378.
- Wells, G. B. (2008) Structural answers and persistent questions about how nicotinic receptors work. *Front. Biosci.* 13, 5479–5510.
- Unwin, N. (2005) Refined structure of the nicotinic acetylcholine receptor at 4 Å resolution. *J. Mol. Biol.* 346, 967–989.
- Hilf, R. J., and Dutzler, R. (2008) X-ray structure of a prokaryotic pentameric ligand-gated ion channel. *Nature* 452, 375–379.
- Hilf, R. J., and Dutzler, R. (2009) Structure of a potentially open state of a proton-activated pentameric ligand-gated ion channel. *Nature* 457, 115–118.
- Bocquet, N., Nury, H., Baaden, M., Le Poupon, C., Changeux, J. P., Delarue, M., and Corringer, P. J. (2009) X-ray structure of a pentameric ligand-gated ion channel in an apparently open conformation. *Nature* 457, 111–114.
- Auerbach, A. (2003) Life at the top: The transition state of AChR gating. *Sci. STKE* 2003, re11.
- Burzomato, V., Beato, M., Groot-Kormelink, P. J., Colquhoun, D., and Sivilotti, L. G. (2004) Single-channel behavior of heteromeric $\alpha 1\beta$ glycine receptors: An attempt to detect a conformational change before the channel opens. *J. Neurosci.* 24, 10924–10940.
- Lape, R., Colquhoun, D., and Sivilotti, L. G. (2008) On the nature of partial agonism in the nicotinic receptor superfamily. *Nature* 454, 722–727.
- Beckstein, O., and Sansom, M. S. (2004) The influence of geometry, surface character, and flexibility on the permeation of ions and water through biological pores. *Phys. Biol.* 1, 42–52.
- Cymes, G. D., and Grosman, C. (2008) Pore-opening mechanism of the nicotinic acetylcholine receptor evinced by proton transfer. *Nat. Struct. Mol. Biol.* 15, 389.
- Auerbach, A., and Akk, G. (1998) Desensitization of mouse nicotinic acetylcholine receptor channels. A two-gate mechanism. *J. Gen. Physiol.* 112, 181–197.
- Karlin, A. (2002) Emerging structure of the nicotinic acetylcholine receptors. *Nat. Rev. Neurosci.* 3, 102–114.
- Purohit, Y., and Grosman, C. (2006) Block of muscle nicotinic receptors by choline suggests that the activation and desensitization gates act as distinct molecular entities. *J. Gen. Physiol.* 127, 703–717.
- Prince, R. J., and Sine, S. M. (1999) Acetylcholine and epibatidine binding to muscle acetylcholine receptors distinguish between concerted and uncoupled models. *J. Biol. Chem.* 274, 19623–19629.
- Bouzat, C., Bartos, M., Corradi, J., and Sine, S. M. (2008) The interface between extracellular and transmembrane domains of homomeric Cys-loop receptors governs open-channel lifetime and rate of desensitization. *J. Neurosci.* 28, 7808–7819.
- Heidmann, T., and Changeux, J. P. (1979) Fast kinetic studies on the allosteric interactions between acetylcholine receptor and local anesthetic binding sites. *Eur. J. Biochem.* 94, 281–296.
- Quast, U., Schimerlik, M. L., and Raftery, M. A. (1979) Ligand-induced changes in membrane-bound acetylcholine receptor observed by ethidium fluorescence. 2. Stopped-flow studies with agonists and antagonists. *Biochemistry* 18, 1891–1901.
- Steinbach, J. H., and Sine, S. M. (1987) Function of nicotinic acetylcholine receptors. *Soc. Gen. Physiol. Ser.* 41, 19–42.
- Forman, S. A., and Miller, K. W. (1988) High acetylcholine concentrations cause rapid inactivation before fast desensitization in nicotinic acetylcholine receptors from *Torpedo*. *Biophys. J.* 54, 149–158.
- Edelstein, S. J., Schaad, O., Henry, E., Bertrand, D., and Changeux, J. P. (1996) A kinetic mechanism for nicotinic acetylcholine receptors based on multiple allosteric transitions. *Biol. Cybernetics* 75, 361–379.
- Muhn, P., Fahr, A., and Hucho, F. (1984) Rapid laser flash photoaffinity labeling of binding sites for a noncompetitive inhibitor of the acetylcholine receptor. *Biochemistry* 23, 2725–2730.
- Cox, R. N., Kaldany, R. R., DiPaola, M., and Karlin, A. (1985) Time-resolved photolabeling by quinacrine azide of a noncompetitive inhibitor site of the nicotinic acetylcholine receptor in a transient, agonist-induced state. *J. Biol. Chem.* 260, 7186–7193.
- Heidmann, T., and Changeux, J. P. (1986) Characterization of the transient agonist-triggered state of the acetylcholine receptor rapidly labeled by the noncompetitive blocker [3 H]chlorpromazine: Additional evidence for the open channel conformation. *Biochemistry* 25, 6109–6113.
- Chiara, D. C., Kloczewiak, M. A., Addona, G. H., Yu, J. A., Cohen, J. B., and Miller, K. W. (2001) Site of resting state inhibition of the nicotinic acetylcholine receptor by a hydrophobic inhibitor. *Biochemistry* 40, 296–304.
- Arevalo, E., Chiara, D. C., Forman, S. A., Cohen, J. B., and Miller, K. W. (2005) Gating-enhanced accessibility of hydrophobic sites within the transmembrane region of the nicotinic acetylcholine receptor's δ -subunit. A time-resolved photolabeling study. *J. Biol. Chem.* 280, 13631–13640.
- Pedersen, S. E., Sharp, S. D., Liu, W. S., and Cohen, J. B. (1992) Structure of the noncompetitive antagonist-binding site of the *Torpedo* nicotinic acetylcholine receptor. [3 H]Meproadifen mustard reacts selectively with α -subunit Glu-262. *J. Biol. Chem.* 267, 10489–10499.
- White, B. H., and Cohen, J. B. (1988) Photolabeling of membrane-bound *Torpedo* nicotinic acetylcholine receptor with the hydrophobic probe 3-trifluoromethyl-3-(m-[125 I]iodophenyl)diazirine. *Biochemistry* 27, 8741–8751.
- Brauer, A. W., Oman, C. L., and Margolies, M. N. (1984) Use of o-phthalaldehyde to reduce background during automated Edman degradation. *Anal. Biochem.* 137, 134–142.
- Middleton, R. E., and Cohen, J. B. (1991) Mapping of the acetylcholine binding site of the nicotinic acetylcholine receptor: [3 H]Nicotine as an agonist photoaffinity label. *Biochemistry* 30, 6987–6997.
- Rankin, S. E., Addona, G. H., Kloczewiak, M. A., Bugge, B., and Miller, K. W. (1997) The cholesterol dependence of activation and fast desensitization of the nicotinic acetylcholine receptor. *Biophys. J.* 73, 2446–2455.
- Maconochie, D. J., and Steinbach, J. H. (1998) The channel opening rate of adult- and fetal-type mouse muscle nicotinic receptors activated by acetylcholine. *J. Physiol.* 506 (Part 1), 53–72.

35. Wu, G., Raines, D. E., and Miller, K. W. (1994) A hydrophobic inhibitor of the nicotinic acetylcholine receptor acts on the resting state. *Biochemistry* 33, 15375–15381.
36. Garcia, G., III, Chiara, D. C., Nirthanan, S., Hamouda, A. K., Stewart, D. S., and Cohen, J. B. (2007) [³H]Benzophenone photolabeling identifies state-dependent changes in nicotinic acetylcholine receptor structure. *Biochemistry* 46, 10296–10307.
37. Blanton, M. P., and Cohen, J. B. (1994) Identifying the lipid-protein interface of the *Torpedo* nicotinic acetylcholine receptor: Secondary structure implications. *Biochemistry* 33, 2859–2872.
38. Hamouda, A. K., Sanghvi, M., Chiara, D. C., Cohen, J. B., and Blanton, M. P. (2007) Identifying the lipid-protein interface of the $\alpha 4\beta 2$ neuronal nicotinic acetylcholine receptor: Hydrophobic photolabeling studies with 3-(trifluoromethyl)-3-(m-[¹²⁵I]iodophenyl)di-azirine. *Biochemistry* 46, 13837–13846.
39. Wilson, G., and Karlin, A. (2001) Acetylcholine receptor channel structure in the resting, open, and desensitized states probed with the substituted-cysteine-accessibility method. *Proc. Natl. Acad. Sci. U.S.A.* 98, 1241–1248.
40. Andreeva, I. E., and Pedersen, S. E. (2005) Conformational asymmetry of nicotinic acetylcholine receptor (AChR) desensitization. *Biophys. J.* 89, 3052.
41. Andreeva, I. E., Nirthanan, S., Cohen, J. B., and Pedersen, S. E. (2006) Site specificity of agonist-induced opening and desensitization of the *Torpedo californica* nicotinic acetylcholine receptor. *Biochemistry* 45, 195–204.
42. Cheng, X., Ivanov, I., Wang, H., Sine, S. M., and McCammon, J. A. (2007) Nanosecond-timescale conformational dynamics of the human $\alpha 7$ nicotinic acetylcholine receptor. *Biophys. J.* 93, 2622–2634.
43. Haddadian, E. J., Cheng, M. H., Coalson, R. D., Xu, Y., and Tang, P. (2008) In silico models for the human $\alpha 4\beta 2$ nicotinic acetylcholine receptor. *J. Phys. Chem. B* 112, 13981–13990.
44. Nirthanan, S., Garcia, G., III, Chiara, D. C., Husain, S. S., and Cohen, J. B. (2008) Identification of binding sites in the nicotinic acetylcholine receptor for TDBzl-etomidate, a photoreactive positive allosteric modulator. *J. Biol. Chem.* 283, 22051–22062.
45. Mihic, S. J., Ye, Q., Wick, M. J., Koltchine, V. V., Krasowski, M. D., Finn, S. E., Mascia, M. P., Valenzuela, C. F., Hanson, K. K., Greenblatt, E. P., Harris, R. A., and Harrison, N. L. (1997) Sites of alcohol and volatile anaesthetic action on GABA(A) and glycine receptors. *Nature* 389, 385–389.
46. Chiara, D. C., Dangott, L. J., Eckenhoff, R. G., and Cohen, J. B. (2003) Identification of nicotinic acetylcholine receptor amino acids photolabeled by the volatile anesthetic halothane. *Biochemistry* 42, 13457–13467.
47. Chiara, D. C., Hong, F. H., Arevalo, E., Husain, S. S., Miller, K. W., Forman, S. A., and Cohen, J. B. (2009) Time-resolved photolabeling of the nicotinic acetylcholine receptor by [³H]azietomidate, an open-state inhibitor. *Mol. Pharmacol.* 75, 1084–1095.
48. Pettersen, E. F., Goddard, T. D., Huang, C. C., Couch, G. S., Greenblatt, D. M., Meng, E. C., and Ferrin, T. E. (2004) UCSF Chimera: A Visualization System for Exploratory Research and Analysis. *J. Comput. Chem.* 25, 1605–1612.